Regularizing Neural Networks via Minimizing Hyperspherical Energy

Rongmei Lin[1], Weiyang Liu[2,*], Zhen Liu[3], Chen Feng[4], Zhiding Yu[5], James M. Rehg[2], Li Xiong[1], Le Song[2]
[1]Emory University [2]Georgia Institute of Technology [3]Mila, Université de Montréal [4]New York University [5]NVIDIA
rongmei.lin@emory.edu wyliu@gatech.edu lxiong@emory.edu lsong@cc.gatech.edu

Abstract

Inspired by the Thomson problem in physics where the distribution of multiple propelling electrons on a unit sphere can be modeled via minimizing some potential energy, hyperspherical energy minimization has demonstrated its potential in regularizing neural networks and improving their generalization power. In this paper, we first study the important role that hyperspherical energy plays in neural network training by analyzing its training dynamics. Then we show that naively minimizing hyperspherical energy suffers from some difficulties due to highly non-linear and non-convex optimization as the space dimensionality becomes higher, therefore limiting the potential to further improve the generalization. To address these problems, we propose the compressive minimum hyperspherical energy (CoMHE) as a more effective regularization for neural networks. Specifically, CoMHE utilizes projection mappings to reduce the dimensionality of neurons and minimizes their hyperspherical energy. According to different designs for the projection mapping, we propose several distinct yet well-performing variants and provide some theoretical guarantees to justify their effectiveness. Our experiments show that CoMHE consistently outperforms existing regularization methods, and can be easily applied to different neural networks.

1. Introduction

Recent years have witnessed the tremendous success of deep neural networks in a variety of tasks. With its over-parameterization nature and hierarchical structure, deep neural networks achieve unprecedented performance on many challenging problems [1, 2, 3], but their strong approximation ability also makes it easy to overfit the training set, which greatly affects the generalization on unseen samples. Therefore, how to restrict the huge parameter space and properly regularize the deep networks becomes increasingly important. Regularizations for neural networks can be roughly categorized into *implicit* and *explicit* ones. Implicit regularizations usually do not directly impose explicit constraints on neuron weights, and instead they regularize the networks in an implicit manner in order to prevent overfitting and stabilize the training. A lot of prevailing methods fall into this category, such as batch normalization [4], dropout [5], weight normalization [6], etc. Explicit regularizations [7, 8, 9, 10, 11, 12] usually introduce some penalty terms for neuron weights, and jointly optimize them along with the other objective functions.

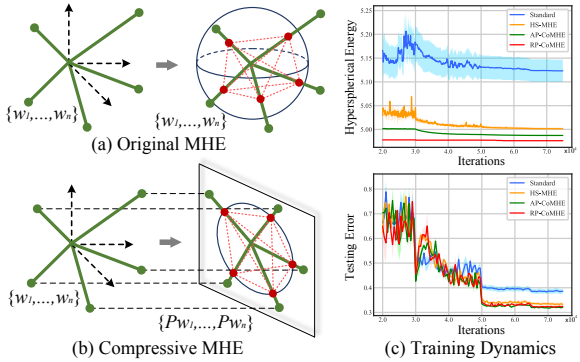

Figure 1: Comparison of original MHE and compressive MHE. In (c), the top figure shows the hyperspherical energy, and the bottom one shows the testing error (CIFAR-100). Experimental details are given in Appendix B.

Among many existing explicit regularizations, minimum hyperspherical energy (MHE) [12] stands out as a simple yet effective regularization that promotes the *hyperspherical diversity* among neurons and significantly improves the network generalization. MHE regularizes the directions of neuron weights by minimizing a potential energy on a unit hypersphere that characterizes the hyperspherical diversity (such energy is defined as *hyperspherical energy* [12]). In contrast, standard weight decay only regularizes the norm of neuron weights, which essentially can be viewed as regularizing one dimension of the weights. MHE completes an important missing piece by regularizing the neuron directions (*i.e.*, regularizing the rest dimensions of the weights).

Although minimizing hyperspherical energy has already been empirically shown useful in a number of applications [12], two fundamental questions remain unanswered: *(1) what is the role that hyperspherical energy plays in training a well-performing neural network?* and *(2) How can the hyperspherical energy be effectively minimized?* To

*Weiyang Liu is the corresponding author.

study the first question, we plot the training dynamics of hyperspherical energy (on CIFAR-100) in Fig. 1(c) for a baseline convolutional neural network (CNN) without any MHE variant, a CNN regularized by MHE [12] and a CNN regularized by our CoMHE. More experimental details and full results (with more interesting baselines) are given in Appendix B. From the empirical results in Fig. 1(c), we find that both MHE and CoMHE can achieve much lower hyperspherical energy and testing error than the baseline, showing the effectiveness of minimizing hyperspherical energy. It also implies that lower hyperspherical energy typically leads to better generalization. We empirically observe that a trained neural network with lower hyperspherical energy often generalizes better (*i.e.*, higher hyperspherical diversity leads to better generalization), and therefore we argue that hyperspherical energy is closely related to the generalization power of neural networks. In the rest of the paper, we delve into the second question that remains an open challenge: how to effectively minimize hyperspherical energy.

By adopting the definition of hyperspherical energy as the regularization objective and naively minimizing it with back-propagation, MHE suffers from a few critical problems which limit it to further unleash its potential. First, the original MHE objective has a huge number of local minima and stationary points due to its highly non-convex and non-linear objective function. The problem can get even worse when the space dimension gets higher and the number of neurons becomes larger [13, 14]. Second, the gradient of the original MHE objective *w.r.t* the neuron weight is deterministic. Unlike the weight decay whose objective is convex, MHE has a complex and non-convex regularization term. Therefore, deterministic gradients may make the solution quickly fall into one of the bad local minima and get stuck there. Third, MHE defines an ill-posed problem in general. When the number of neurons is smaller than the dimension of the space (it is often the case in neural networks), it will be less meaningful to encourage the hyperspherical diversity since the neurons can not fully occupy the space. Last, in high-dimensional spaces, randomly initialized neurons are likely to be orthogonal to each other (see Appendix C). Therefore, these high-dimensional neurons can be trivially "diverse", leading to small gradients in original MHE that cause optimization difficulties.

In order to address these problems and effectively minimize hyperspherical energy, we propose the compressive minimum hyperspherical energy (CoMHE) as a generic regularization for neural networks. The high-level intuition behind CoMHE is to project neurons to some suitable subspaces such that the hyperspherical energy can get minimized more effectively. Specifically, CoMHE first maps the neurons from a high-dimensional space to a low-dimensional one and then minimizes the hyperspherical energy of these neurons. Therefore, how to map these neurons to a low-dimensional space while preserving the desirable information in high-dimensional space is our major concern. Since we aim to regularize the directions of neurons, what we care most is the angular similarity between different neurons. To this end, we explore multiple novel methods to perform the projection and heavily study two main approaches: *random projection* and *angle-preserving projection*, which can reduce the dimensionality of neurons while still partially preserving the pairwise angles.

Random projection (RP) is a natural choice to perform the dimensionality reduction in MHE due to its simplicity and nice theoretical properties. RP can provably preserve the angular information, and most importantly, introduce certain degree of randomness to the gradients, which may help CoMHE escape from some bad local minima. The role that the randomness serves in CoMHE is actually similar to the *simulated annealing* [15, 16] that is widely used to solve Thomson problem. Such randomness is often shown to benefit the generalization [17, 18]. We also provably show that using RP can well preserve the pairwise angles between neurons. Besides RP, we propose the angle-preserving projection (AP) as an effective alternative. AP is motivated by the goal that we aim to preserve the pairwise angles between neurons. Constructing an AP that can project neurons to a low-dimensional space that well preserves the angles is often difficult even with powerful non-linear functions, which is suggested by the strong conditions required for conformal mapping in complex analysis [19]. Therefore, we frame the AP construction as an optimization problem which can be solved jointly with hyperspherical energy minimization. More interestingly, we consider the *adversarial projection* for CoMHE, which minimizes the maximal energy attained by learning the projection. We formulate it as a min-max optimization and optimize it jointly with the neural network.

However, it is inevitable to lose some information in low-dimensional spaces and the neurons may only get diverse in some particular low-dimensional spaces. To address it, we adopt multiple projections to better approximate the MHE objective in the original high-dimensional space. Specifically, we project the neurons to multiple subspaces, compute the hyperspherical energy in each space separately and then minimize the aggregation (*i.e.*, average or max). Moreover, we reinitialize these projection matrix randomly every certain number of iterations to avoid trivial solutions.

In contrast to MHE that imposes a static regularization to the neurons, CoMHE dynamically regularizes the neurons based on the projection matrices. Such dynamic regularization is equivalent to adjusting the CoMHE objective function, making it easier to escape some bad local minima. Our contributions can be summarized as:

- We first show that hyperspherical energy is closely related to generalization and then reveal the role it plays in training a neural network that generalizes well.

- To address the drawbacks of MHE, we propose CoMHE as a dynamic regularization to effectively minimize hyperspherical energy of neurons for better generalizability.
- We explore different ways to construct a suitable projection for CoMHE. Random projection and angle-preserving projection are proposed to reduce the dimensionality of neurons while preserving the angular information. We also consider several variants such as adversarial projection CoMHE and group CoMHE.
- We provide some theoretical insights for the proposed projections on the quality of preserving the angular similarity between different neurons.
- We show that CoMHE consistently outperforms the original MHE in different tasks. Notably, a 9-layer plain CNN regularized by CoMHE outperforms a standard 1001-layer ResNet by more than 2% on CIFAR-100.

2. Related Work

Diversity-based regularization has been found useful in sparse coding [20, 21], ensemble learning [22, 23], self-paced learning [24], metric learning [25], latent variable models [26], etc. Early studies in sparse coding [20, 21] model the diversity with the empirical covariance matrix and show that encouraging such diversity can improve the dictionary's generalizability. [27] promotes the uniformity among eigenvalues of the component matrix in a latent space model. [28, 29, 30, 9, 8, 30] characterize diversity among neurons with orthogonality, and regularize the neural network by promoting the orthogonality. Inspired by the Thomson problem in physics, MHE [12] defines the hyperspherical energy to characterize the diversity on a unit hypersphere and shows significant and consistent improvement in supervised learning tasks. There are two MHE variants in [12]: full-space MHE and half-space MHE. Compared to full-space MHE, the half-space variant [12] further eliminates the collinear redundancy by constructing virtual neurons with the opposite direction to the original ones and then minimizing their hyperspherical energy together. The importance of regularizing angular information is also discussed in [31, 32, 33, 34, 35, 36, 37, 38, 39, 40].

3. Compressive MHE

3.1. Revisiting Standard MHE

MHE characterizes the diversity of N neurons ($\boldsymbol{W}_N = \{\boldsymbol{w}_1, \cdots, \boldsymbol{w}_N \in \mathbb{R}^{d+1}\}$) on a unit hypersphere using hyperspherical energy which is defined as

$$\begin{aligned} \boldsymbol{E}_{s,d}(\hat{\boldsymbol{w}}_i|_{i=1}^N) &= \sum_{i=1}^N \sum_{j=1,j\neq i}^N f_s(\|\hat{\boldsymbol{w}}_i - \hat{\boldsymbol{w}}_j\|) \\ &= \begin{cases} \sum_{i\neq j} \|\hat{\boldsymbol{w}}_i - \hat{\boldsymbol{w}}_j\|^{-s}, & s>0 \\ \sum_{i\neq j} \log\left(\|\hat{\boldsymbol{w}}_i - \hat{\boldsymbol{w}}_j\|^{-1}\right), & s=0 \end{cases} \end{aligned} \tag{1}$$

where $\|\cdot\|$ denotes ℓ_2 norm, $f_s(\cdot)$ is a decreasing real-valued function (we use $f_s(z)=z^{-s}, s>0$, *i.e.*, Riesz s-kernels), and $\hat{\boldsymbol{w}}_i = \frac{\boldsymbol{w}_i}{\|\boldsymbol{w}_i\|}$ is the i-th neuron weight projected onto the unit hypersphere $\mathbb{S}^d = \{\boldsymbol{v}\in\mathbb{R}^{d+1} \,|\, \|\boldsymbol{v}\|=1\}$. For convenience, we denote $\hat{\boldsymbol{W}}_N = \{\hat{\boldsymbol{w}}_1, \cdots, \hat{\boldsymbol{w}}_N \in \mathbb{S}^d\}$, and $\boldsymbol{E}_s = \boldsymbol{E}_{s,d}(\hat{\boldsymbol{w}}_i|_{i=1}^N)$. Note that, each neuron is a convolution kernel in CNNs. MHE minimizes the hyperspherical energy of neurons using gradient descent during back-propagation, and MHE is typically applied to the neural network in a layer-wise fashion. We first write down the gradient of $\boldsymbol{E}_2$ *w.r.t* $\hat{\boldsymbol{w}}_i$ and make the gradient to be zero:

$$\nabla_{\hat{\boldsymbol{w}}_i} \boldsymbol{E}_2 = \sum_{j=1,j\neq i}^N \frac{-2(\hat{\boldsymbol{w}}_i - \hat{\boldsymbol{w}}_j)}{\|\hat{\boldsymbol{w}}_i - \hat{\boldsymbol{w}}_j\|^4} = 0 \Rightarrow \hat{\boldsymbol{w}}_i = \frac{\sum_{j=1,j\neq i}^N \alpha_j \hat{\boldsymbol{w}}_j}{\sum_{j=1,j\neq i}^N \alpha_j} \tag{2}$$

where $\alpha_j = \|\hat{\boldsymbol{w}}_i - \hat{\boldsymbol{w}}_j\|^{-4}$. We use toy and informal examples to show that high dimensional space (*i.e.*, d is large) leads to much more stationary points than low-dimensional one. Assume there are $K = K_1 + K_2$ stationary points in total for $\hat{\boldsymbol{W}}_N$ to satisfy Eq. 2, where K_1 denotes the number of stationary points in which every element in the solution is distinct and K_2 denotes the number of the rest stationary points. We give two examples: *(i)* For $(d+2)$-dimensional space, we can extend the solutions in $(d+1)$-dimensional space by introducing a new dimension with zero value. The new solutions satisfy Eq. 2. Because there are $d+2$ ways to insert the zero, we have at least $(d+2)K$ stationary points in $(d+2)$-dimensional space. *(ii)* We denote $K_1' = \frac{K_1}{(d+1)!}$ as the number of unordered sets that construct the stationary points. In $(2d+2)$-dimensional space, we can construct $\hat{\boldsymbol{w}}_j^E = \frac{1}{\sqrt{2}}\{\hat{\boldsymbol{w}}_j; \hat{\boldsymbol{w}}_j\} \in \mathbb{S}^{2d+1}, \forall j$ that satisfies Eq. 2. Therefore, there are at least $\frac{(2d+2)!}{2^{d+1}} K_1' + K_2$ stationary points for $\hat{\boldsymbol{W}}_N$ in $(2d+2)$-dimensional space, and besides this construction, there are much more stationary points. Therefore, MHE have far more stationary points in higher dimensions.

3.2. General Framework

To overcome MHE's drawbacks in high dimensional space, we propose the compressive MHE that projects the neurons to a low-dimensional space and then minimizes the hyperspherical energy of the projected neurons. In general, CoMHE minimizes the following form of energy:

$$\boldsymbol{E}_s^C(\hat{\boldsymbol{W}}_N) := \sum_{i=1}^N \sum_{j=1,j\neq i}^N f_s\Big(\|g(\hat{\boldsymbol{w}}_i) - g(\hat{\boldsymbol{w}}_j)\|\Big) \tag{3}$$

where $g: \mathbb{S}^d \to \mathbb{S}^k$ takes a normalized $(d+1)$-dimensional input and outputs a normalized $(k+1)$-dimensional vector. $g(\cdot)$ can be either linear or nonlinear mapping. We only consider the linear case here. Using multi-layer perceptrons as $g(\cdot)$ is one of the simplest nonlinear cases. Similar to MHE, CoMHE also serves as a regularization in neural networks.

3.3. Random Projection for CoMHE

Random projection is in fact one of the most straightforward way to reduce dimensionality while partially preserving the angular information. More specifically, we use a

random mapping $g(\boldsymbol{v}) = \frac{\boldsymbol{P}\boldsymbol{v}}{\|\boldsymbol{P}\boldsymbol{v}\|}$ where $\boldsymbol{P} \in \mathbb{R}^{(k+1)\times(d+1)}$ is a Gaussian distributed random matrix (each entry follows i.i.d. normal distribution). In order to reduce the variance, we use C random projection matrices to project the neurons and compute the hyperspherical energy separately:

$$\boldsymbol{E}_s^R(\hat{\boldsymbol{W}}_N) := \frac{1}{C}\sum_{c=1}^{C}\sum_{i=1}^{N}\sum_{j=1,j\neq i}^{N} f_s\Big(\Big\|\frac{\boldsymbol{P}_c\hat{\boldsymbol{w}}_i}{\|\boldsymbol{P}_c\hat{\boldsymbol{w}}_i\|} - \frac{\boldsymbol{P}_c\hat{\boldsymbol{w}}_j}{\|\boldsymbol{P}_c\hat{\boldsymbol{w}}_j\|}\Big\|\Big) \quad (4)$$

where $\boldsymbol{P}_c, \forall c$ is a random matrix with each entry following the normal distribution $\mathcal{N}(0,1)$. According to the properties of normal distribution [41], every normalized row of the random matrix $\boldsymbol{P}$ is uniformly distributed on a hypersphere $\mathbb{S}^d$, which indicates that the projection matrix $\boldsymbol{P}$ is able to cover all the possible subspaces. Multiple projection matrices can also be interpreted as multi-view projection, because we are making use of information from multiple projection views. In fact, we do not necessarily need to average the energy for multiple projections, and instead we can use maximum operation (or some other meaningful aggregation operations). Then the objective becomes $\max_c \sum_{i=1}^{N}\sum_{j=1,j\neq i}^{N} f_s(\|\frac{\boldsymbol{P}_c\hat{\boldsymbol{w}}_i}{\|\boldsymbol{P}_c\hat{\boldsymbol{w}}_i\|} - \frac{\boldsymbol{P}_c\hat{\boldsymbol{w}}_j}{\|\boldsymbol{P}_c\hat{\boldsymbol{w}}_j\|}\|)$. Considering that we aim to minimize this objective, the problem is in fact a min-max optimization. Note that, we will typically re-initialize the random projection matrices every certain number of iterations to avoid trivial solutions. Most importantly, using RP can provably preserve the angular similarity.

3.4. Angle-preserving Projection for CoMHE

Recall that we aim to find a projection to project the neurons to a low-dimensional space that best preserves angular information. We transform the goal to an optimization:

$$\boldsymbol{P}^\star = \arg\min_{\boldsymbol{P}} \mathcal{L}_P := \sum_{i\neq j}(\theta_{(\hat{\boldsymbol{w}}_i,\hat{\boldsymbol{w}}_j)} - \theta_{(\boldsymbol{P}\hat{\boldsymbol{w}}_i,\boldsymbol{P}\hat{\boldsymbol{w}}_j)})^2 \quad (5)$$

where $\boldsymbol{P} \in \mathbb{R}^{(k+1)\times(d+1)}$ is the projection matrix and $\theta_{(\boldsymbol{v}_1,\boldsymbol{v}_2)}$ denotes the angle between $\boldsymbol{v}_1$ and $\boldsymbol{v}_2$. For implementation convenience, we can replace the angle with the cosine value (*e.g.*, use $\cos(\theta_{(\hat{\boldsymbol{w}}_i,\hat{\boldsymbol{w}}_j)})$ to replace $\theta_{(\hat{\boldsymbol{w}}_i,\hat{\boldsymbol{w}}_j)}$), so that we can directly use the inner product of normalized vectors to measure the angular similarity. With $\hat{\boldsymbol{P}}$ obtained in Eq. 5, we use a nested loss function:

$$\begin{aligned}\boldsymbol{E}_s^A(\hat{\boldsymbol{W}}_N, \boldsymbol{P}^\star) &:= \sum_{i=1}^{N}\sum_{j=1,j\neq i}^{N} f_s\Big(\Big\|\frac{\boldsymbol{P}^\star\hat{\boldsymbol{w}}_i}{\|\boldsymbol{P}^\star\hat{\boldsymbol{w}}_i\|} - \frac{\boldsymbol{P}^\star\hat{\boldsymbol{w}}_j}{\|\boldsymbol{P}^\star\hat{\boldsymbol{w}}_j\|}\Big\|\Big) \\ \text{s.t.}\quad \boldsymbol{P}^\star &= \arg\min_{\boldsymbol{P}}\sum_{i\neq j}(\theta_{(\hat{\boldsymbol{w}}_i,\hat{\boldsymbol{w}}_j)} - \theta_{(\boldsymbol{P}\hat{\boldsymbol{w}}_i,\boldsymbol{P}\hat{\boldsymbol{w}}_j)})^2\end{aligned} \quad (6)$$

for which we propose two different ways to optimize the projection matrix $\boldsymbol{P}$. We can approximate $\boldsymbol{P}^\star$ using a few gradient descent updates. Specifically, we use two different ways to perform the optimization. Naively, we use a few gradient descent steps to update $\boldsymbol{P}$ in order to approximate $\boldsymbol{P}^\star$ and then update $\boldsymbol{W}_N$, which proceeds alternately. The number of iteration steps that we use to update $\boldsymbol{P}$ is a hyperparemter and needs to be determined by cross-validation. Besides the naive alternate one, we also use a different optimization of $\boldsymbol{W}_N$ by unrolling the gradient update of $\boldsymbol{P}$.

Alternating optimization. The alternating optimization is to optimize $\boldsymbol{P}$ alternately with the network parameters $\boldsymbol{W}_N$. Specifically, in each iteration of updating the network parameters, we update $\boldsymbol{P}$ every number of inner iterations and use it as an approximation to $\boldsymbol{P}^\star$ (the error depends on the number of gradient steps we take). Essentially, we are alternately solving two separate optimization problems for $\boldsymbol{P}$ and $\boldsymbol{W}_N$ with gradient descent.

Unrolled optimization. Instead of naively updating $\boldsymbol{W}_N$ with approximate $\boldsymbol{P}^\star$ in the alternating optimization, the unrolled optimization further unrolls the update rule of $\boldsymbol{P}$ and embed it within the optimization of network parameters $\boldsymbol{W}_N$. If we denote the CoMHE loss with a given projection matrix $\boldsymbol{P}$ as $\boldsymbol{E}_s^A(\boldsymbol{W}_N, \boldsymbol{P})$ which takes $\boldsymbol{W}_N$ and $\boldsymbol{P}$ as input, then the unrolled optimization is essentially optimizing $\boldsymbol{E}_s^A(\boldsymbol{W}_N, \boldsymbol{P} - \eta\cdot\frac{\partial\mathcal{L}_P}{\partial\boldsymbol{P}})$. It can also be viewed as minimizing the CoMHE loss after a single step of gradient descent *w.r.t.* the projection matrix. This optimization includes the computation of second-order partial derivatives. Note that, it is also possible to unroll multiple gradient descent steps. Similar unrolling is also applied in [42, 43, 44].

3.5. Notable CoMHE Variants

We provide more interesting CoMHE variants as an extension. We will have some preliminary empirical study on these variants, but our main focus is still on RP and AP.

Adversarial Projection for CoMHE. We consider a novel CoMHE variant that adversarially learns the projection. The intuition behind is that we want to learn a projection basis that maximizes the hyperspherical energy while the final goal is to minimize this maximal energy. With such intuition, we can construct a min-max optimization:

$$\min_{\hat{\boldsymbol{W}}_N}\max_{\boldsymbol{P}} \boldsymbol{E}_s^V(\hat{\boldsymbol{W}}_N, \boldsymbol{P}) := \sum_{i=1}^{N}\sum_{j=1,j\neq i}^{N} f_s\Big(\Big\|\frac{\boldsymbol{P}\hat{\boldsymbol{w}}_i}{\|\boldsymbol{P}\hat{\boldsymbol{w}}_i\|} - \frac{\boldsymbol{P}\hat{\boldsymbol{w}}_j}{\|\boldsymbol{P}\hat{\boldsymbol{w}}_j\|}\Big\|\Big) \quad (7)$$

which can be solved by gradient descent similar to [45]. From a game-theoretical perspective, $\boldsymbol{P}$ and $\hat{\boldsymbol{W}}_N$ can be viewed as two players that are competing with each other. However, due to the instability of solving the min-max problem, the performance of this projection is unstable.

Group CoMHE. Group CoMHE is a very special case in the CoMHE framework. The basic idea is to divide the weights of each neuron into several groups and then minimize the hyperspherical energy within each group. For example in CNNs, group MHE divides the channels into groups and minimizes within each group the MHE loss. Specifically, the objective function of group CoMHE is

$$\boldsymbol{E}_s^G(\hat{\boldsymbol{W}}_N) := \frac{1}{C}\sum_{c=1}^{C}\sum_{i=1}^{N}\sum_{j=1,j\neq i}^{N} f_s\Big(\Big\|\frac{\boldsymbol{P}_c\hat{\boldsymbol{w}}_i}{\|\boldsymbol{P}_c\hat{\boldsymbol{w}}_i\|} - \frac{\boldsymbol{P}_c\hat{\boldsymbol{w}}_j}{\|\boldsymbol{P}_c\hat{\boldsymbol{w}}_j\|}\Big\|\Big) \quad (8)$$

where $\boldsymbol{P}_c$ is a diagonal matrix with every diagonal entry being either 0 or 1, and $\sum_c \boldsymbol{P}_c = \boldsymbol{I}$ (in fact, this is optional).

There are multiple ways to divide groups for the neurons, and typically we will divide groups according to the channels, similar to [46]. More interestingly, one can also divide the groups in a *stochastic* fashion.

3.6. Shared Projection Basis in Neural Networks

In general, we usually need different projection bases for neurons in different layers of the neural network. However, we find it beneficial to share some projection bases across different layers. We only share the projection matrix for the neurons in different layers that have the same dimensionality. For example in a neural network, if the neurons in the first layer have the same dimensionality with the neurons in the second layer, we will share their projection matrix that reduces the dimensionality. Sharing the projection basis can effectively reduce the number of projection parameters and may also reduce the inconsistency within the hyperspherical energy minimization of projected neurons in different layers. Most importantly, it can empirically improve the network generalizability while using much fewer parameters and saving more computational overheads.

4. Theoretical Insights

4.1. Angle Preservation

We start with highly relevant properties of random projection and then delve into the angular preservation.

Lemma 1 (Mean Preservation of Random Projection)**.** *For any $\boldsymbol{w}_1, \boldsymbol{w}_2 \in \mathbb{R}^d$ and any random Gaussian distributed matrix $\boldsymbol{P} \in \mathbb{R}^{k\times d}$ where $\boldsymbol{P}_{ij} = \frac{1}{\sqrt{n}} r_{ij}$, if $r_{ij}, \forall i, j$ are i.i.d. random variables from $\mathcal{N}(0,1)$, we have $\mathbb{E}(\langle \boldsymbol{P}\boldsymbol{w}_1, \boldsymbol{P}\boldsymbol{w}_2\rangle) = \langle \boldsymbol{w}_1, \boldsymbol{w}_2\rangle$.*

This lemma indicates that the mean of randomly projected inner product is well preserved, partially justifying why using random projection actually makes senses.

Johnson-Lindenstrauss lemma (JLL) [47, 48] (in Appendix D) establishes a guarantee for the Euclidean distance between randomly projected vectors. However, JLL does not provide the angle preservation guarantees. It is nontrivial to provide a guarantee for angular similarity from JLL.

Theorem 1 (Angle Preservation I)**.** *Given $\boldsymbol{w}_1, \boldsymbol{w}_2 \in \mathbb{R}^d$, $\boldsymbol{P} \in \mathbb{R}^{k\times d}$ is a random projection matrix that has i.i.d. 0-mean σ-subgaussian entries, and $\boldsymbol{P}\boldsymbol{w}_1, \boldsymbol{P}\boldsymbol{w}_2 \in \mathbb{R}^k$ are the randomly projected vectors of $\boldsymbol{w}_1, \boldsymbol{w}_2$ under $\boldsymbol{P}$. Then $\forall \epsilon \in (0,1)$, we have that*

$$\frac{\cos(\theta_{(\boldsymbol{w}_1,\boldsymbol{w}_2)}) - \epsilon}{1+\epsilon} < \cos(\theta_{(\boldsymbol{P}\boldsymbol{w}_1,\boldsymbol{P}\boldsymbol{w}_2)}) < \frac{\cos(\theta_{(\boldsymbol{w}_1,\boldsymbol{w}_2)}) + \epsilon}{1-\epsilon} \tag{9}$$

which holds with probability $\left(1 - 2\exp(-\frac{k\epsilon^2}{8})\right)^2$.

Theorem 2 (Angle Preservation II)**.** *Given $\boldsymbol{w}_1, \boldsymbol{w}_2 \in \mathbb{R}^d$, $\boldsymbol{P} \in \mathbb{R}^{k\times d}$ is a Gaussian random projection matrix where $\boldsymbol{P}_{ij} = \frac{1}{\sqrt{n}} r_{ij}$ ($r_{ij}, \forall i, j$ are i.i.d. random variables from $\mathcal{N}(0,1)$), and $\boldsymbol{P}\boldsymbol{w}_1, \boldsymbol{P}\boldsymbol{w}_2 \in \mathbb{R}^k$ are the randomly projected vectors of $\boldsymbol{w}_1, \boldsymbol{w}_2$ under $\boldsymbol{P}$. Then $\forall \epsilon \in (0,1)$ and $\boldsymbol{w}_1^\top \boldsymbol{w}_2 > 0$, we have that*

$$\begin{aligned} \frac{1+\epsilon}{1-\epsilon}\cos(\theta_{(\boldsymbol{w}_1,\boldsymbol{w}_2)}) - \frac{2\epsilon}{1-\epsilon} &< \cos(\theta_{(\boldsymbol{P}\boldsymbol{w}_1,\boldsymbol{P}\boldsymbol{w}_2)}) \\ &< \frac{1-\epsilon}{1+\epsilon}\cos(\theta_{(\boldsymbol{w}_1,\boldsymbol{w}_2)}) + \frac{1+2\epsilon}{1+\epsilon} - \frac{\sqrt{(1-\epsilon^2)}}{1+\epsilon} \end{aligned} \tag{10}$$

which holds with probability $1 - 6\exp(-\frac{k}{2}(\frac{\epsilon^2}{2} - \frac{\epsilon^3}{3}))$.

Theorem 1 is one of our main theoretical results and reveals that the angle between randomly projected vectors is well preserved. Note that, the parameter σ of the subgaussian distribution is not related to our bound for the angle, so any Gaussian distributed random matrix has the property of angle preservation. The projection dimension k is related to the probability that the angle preservation bound holds. Theorem 2 is a direct result from [49]. It again shows that the angle between randomly projected vectors is provably preserved. Both Theorem 1 and Theorem 2 give upper and lower bounds for the angle between randomly projected vectors. If $\theta_{(\boldsymbol{w}_1,\boldsymbol{w}_2)} > \arccos(\frac{\epsilon+3\epsilon^2}{3\epsilon+\epsilon^2})$, then the lower bound in Theorem 1 is tighter than the lower bound in Theorem 2. If $\theta_{(\boldsymbol{w}_1,\boldsymbol{w}_2)} > \arccos(\frac{1-3\epsilon^2-(1-\epsilon)\sqrt{1-\epsilon^2}}{3\epsilon-\epsilon^2})$, the upper bound in Theorem 1 is tighter than the upper bound in Theorem 2. To conclude, Theorem 1 gives tighter bounds when the angle of original vectors is large. Since AP is randomly initialized every certain number of iterations and minimizes the angular difference before and after the projection, AP usually performs better than RP in preserving angles. Without the angle-preserving optimization, AP reduces to RP.

4.2. Statistical Insights

We can also draw some theoretical intuitions from spherical uniform testing [50] in statistics. Spherical uniform testing is a nonparametric statistical hypothesis test that checks whether a set of observed data is generated from a uniform distribution on a hypersphere or not. Random projection is in fact an important tool [50] in statistics to test the uniformity on hyperspheres, while our goal is to promote the same type of hyperspherical uniformity (*i.e.*, diversity). Specifically, we have N random samples $\boldsymbol{w}_1, \cdots, \boldsymbol{w}_N$ of $\mathbb{S}^d$-valued random variables, and the random projection $\boldsymbol{p}$ which is another random variable independent of $\boldsymbol{w}_i, \forall i$ and uniformly distributed on $\mathbb{S}^d$. The projected points of $\boldsymbol{w}_i, \forall i$ is $y_i = \boldsymbol{p}^\top \boldsymbol{w}_i, \forall i$. The distribution of $y_i, \forall i$ uniquely determines the distribution of $\boldsymbol{w}_1$, as is specified by Theorem 3.

Theorem 3 (Unique Distribution Determination of Random Projection)**.** *Let $\boldsymbol{w}$ be a $\mathbb{S}^d$-valued random variable and $\boldsymbol{p}$ be a random variable that is uniformly distributed on $\mathbb{S}^d$ and independent of $\boldsymbol{w}$. With probability one, the distribution of $\boldsymbol{w}$ is uniquely determined by the distribution of the projection of $\boldsymbol{w}$ on $\boldsymbol{p}$. More specifically, if $\boldsymbol{w}_1$ and $\boldsymbol{w}_2$ are $\mathbb{S}^d$-valued random variables, independent of $\boldsymbol{p}$ and we have*

a positive probability for the event that $\boldsymbol{p}$ takes a value $\boldsymbol{p}_0$ such that the two distributions satisfy $\boldsymbol{p}_0^\top \boldsymbol{w}_1 \sim \boldsymbol{p}_0^\top \boldsymbol{w}_2$, then $\boldsymbol{w}_1$ and $\boldsymbol{w}_2$ are identically distributed.

Theorem 3 shows that the distributional information is well preserved after random projection, providing the CoMHE framework a statistical intuition and foundation. We emphasize that the randomness here is in fact very crucial. For a fixed projection $\boldsymbol{p}_0$, Theorem 3 does not hold in general. As a result, random projection for CoMHE is well motivated from the statistical perspective.

4.3. Insights from Random Matrix Theory

Random projection may also impose some implicit regularization to learning the neuron weights. [51] proves that random projection serves as a regularizer for the Fisher linear discrimination classifier. From metric learning perspective, the inner product between neurons $\boldsymbol{w}_1^\top \boldsymbol{w}_2$ will become $\boldsymbol{w}_1^\top \boldsymbol{P}^\top \boldsymbol{P} \boldsymbol{w}_2$ where $\boldsymbol{P}^\top \boldsymbol{P}$ defines a specific form of (low-rank) similarity [52, 39]. [53] proves that random projection satisfying the JLL *w.h.p* also satisfies the restricted isometry property (RIP) *w.h.p* under sparsity assumptions. In this case, the neuron weights can be well recovered [54, 55]. These results imply that randomly projected neurons in CoMHE may implicitly regularize the network.

5. Discussions and Extensions

Bilateral projection for CoMHE. If we view the neurons in one layer as a matrix $\boldsymbol{W} = \{\boldsymbol{w}_1, \cdots, \boldsymbol{w}_n\} \in \mathbb{R}^{m \times n}$ where m is the dimension of neurons and n is the number of neurons, then the projection considered throughout the paper is to left-multiply a projection matrix $\boldsymbol{P}_1 \in \mathbb{R}^{r \times m}$ to $\boldsymbol{W}$. In fact, we can further reduce the number of neurons by right-multiplying an additional projection matrix $\boldsymbol{P}_2 \in \mathbb{R}^{n \times r}$ to $\boldsymbol{W}$. Specifically, we denote that $\boldsymbol{Y}_1 = \boldsymbol{P}_1 \boldsymbol{W}$ and $\boldsymbol{Y}_2 = \boldsymbol{W} \boldsymbol{P}_2$. Then we can apply the MHE regularization separately to column vectors of $\boldsymbol{Y}_1$ and $\boldsymbol{Y}_2$. The final neurons are still $\boldsymbol{W}$. More interestingly, we can also approximate $\boldsymbol{W}$ with a low-rank factorization [56]: $\tilde{\boldsymbol{W}} = \boldsymbol{Y}_2 (\boldsymbol{P}_1 \boldsymbol{Y}_2)^{-1} \boldsymbol{Y}_1 \in \mathbb{R}^{m \times n}$. It inspires us to directly use two set of parameters $\boldsymbol{Y}_1$ and $\boldsymbol{Y}_2$ to represent the equivalent neurons $\tilde{\boldsymbol{W}}$ and apply the MHE regularization separately to their column vectors. Different from the former case, we use $\tilde{\boldsymbol{W}}$ as the final neurons. More details are in Appendix F.

Constructing random projection matrices. In random projection, we typically construct random matrices with each element drawn *i.i.d.* from a normal distribution. However, there are many more choices for constructing a random matrices that can provably preserve distance information. For example, we have subsampled randomized Hadamard transform [57] and count sketch-based projections [58].

Comparison to existing works. One of the widely used regularizations is the orthonormal regularization [32, 59] that minimizes $\|\boldsymbol{W}^\top \boldsymbol{W} - \boldsymbol{I}\|_F$ where W denotes the weights of a group of neurons with each column being one neuron and $\boldsymbol{I}$ is an identity matrix. [9, 29] are also built upon orthogonality. In contrast, both MHE and CoMHE do not encourage orthogonality among neurons and instead promote hyperspherical uniformity and diversity.

Randomness improves generalization. Both RP and AP introduce randomness to CoMHE, and the empirical results show that such randomness can greatly benefit the network generalization. It is well-known that stochastic gradient is one of the key ingredients that help neural networks generalize well to unseen samples. Interestingly, randomness in CoMHE also leads to a stochastic gradient. [17] also theoretically shows that randomness helps generalization, partially justifying the effectiveness of CoMHE.

6. Experiments and Results

6.1. Image Recognition

We perform image recognition to show the improvement of regularizing CNNs with CoMHE. Our goal is to show the superiority of CoMHE rather than achieving state-of-the-art accuracies on particular tasks. For all the experiments on CIFAR-10 and CIFAR-100 in the paper, we use the same data augmentation as [1, 34]. For ImageNet-2012, we use the same data augmentation in [32]. We train all the networks using SGD with momentum 0.9. All the networks use BN [4] and ReLU if not otherwise specified. By default, all CoMHE variants are built upon half-space MHE. Experimental details are given in each subsection and Appendix A. More experiments are given in Appendix I,H,J.

6.1.1 Ablation Study and Exploratory Experiments

Variants of CoMHE. We compare different variants of CoMHE with the same plain CNN-9 (Appendix A). Specifically, we evaluate the baseline CNN without any regularization, half-space MHE (HS-MHE) which is the best MHE variant from [12], random projection CoMHE (RP-CoMHE), RP-CoMHE (max) that uses max instead of average for loss aggregation, angle-preserving projection CoMHE (AP-CoMHE), adversarial projection CoMHE (Adv-CoMHE) and group CoMHE (G-CoMHE) on CIFAR-100. For RP, we set the projection dimension to 30 (*i.e.*, $k = 29$) and the number of projection to 5 (*i.e.*, $C = 5$). For AP, the number of projection is 1 and the projection dimension is set to 30. For AP, we evaluate both alternating optimization and unrolled optimization. In alternating optimization, we update the projection matrix every 10 steps of network update. In unrolled optimization, we only unroll one-step gradient in the opti-

Method	Error (%)
Baseline	28.03
Orthogonal	27.01
SRIP [9]	25.80
MHE [12]	26.75
HS-MHE [12]	25.96
G-CoMHE	25.08
Adv-CoMHE	25.09
RP-CoMHE	24.39
RP-CoMHE (max)	24.77
AP-CoMHE (alter.)	24.95
AP-CoMHE (unroll)	**24.33**

Table 1: CoMHE variants on C-100.

mization. For G-CoMHE, we construct a group with every 8 consecutive channels. All these design choices are obtained using cross-validation. We will also study how these hyperparameters affect the performance in the following experiments. The results in Table 1 show that all of our proposed CoMHE variants can outperform the original half-space MHE by a large margin. The unrolled optimization in AP-CoMHE shows the significant advantage over alternating one and achieves the best accuracy. Both Adv-CoMHE and G-CoMHE achieve decent performance gain over HS-MHE, but not as good as RP-CoMHE and AP-CoMHE. Therefore, we will mostly focus on RP-CoMHE and AP-CoMHE in the remaining experiments.

Projection Dimension	10	20	30	40	80
RP-CoMHE	25.48	25.32	24.60	**24.75**	25.46
AP-CoMHE (alter.)	**25.21**	24.60	24.95	24.97	**24.99**
AP-CoMHE (unroll.)	25.32	**24.59**	**24.33**	24.93	25.12

Table 2: Error (%) on CIFAR-100 under different dimension of projection.

Dimension of projection. We evaluate how the dimension of projection (*i.e.*, k) affects the performance. We use the plain CNN-9 as the backbone network and test on CIFAR-100. We fix the number of projections in RP-CoMHE to 20. Because AP-CoMHE does not need to use multiple projections to reduce variance, we only use one projection in AP-CoMHE. Results are given in Table 2. In general, RP-CoMHE and AP-CoMHE with different projection dimensions can consistently and significantly outperform the half-space MHE, validating the effectiveness and superiority of the proposed CoMHE framework. Specifically, we find that both RP-CoMHE and AP-CoMHE usually achieve the best accuracy when the projection dimension is 20 or 30. Since the unrolled optimization in AP-CoMHE is consistently better than the alternating optimization, we stick to the unrolled optimization for AP-CoMHE in the remaining experiments if not otherwise specified.

Number of projections. We evaluate RP-CoMHE under different numbers of projections. We use the plain CNN-9 as the baseline and test on CIFAR-100. Results in Table 3 show that the performance of RP-CoMHE is generally not very sensitive to the number of projections. Surprisingly, we find that it is not necessarily better to use more projections for variance reduction. Our experiment show that using 5 projections can achieve the best accuracy. It may be because large variance can help the solution escape bad local minima in the optimization. Note that, we generally do not use multiple projections in AP-CoMHE, because AP-CoMHE optimizes the projection and variance reduction is unnecessary. Our results do not show performance gain by using multiple projections in AP-CoMHE.

# Proj.	RP-CoMHE	AP-CoMHE
1	25.11	**24.33**
5	**24.39**	24.34
10	25.11	24.36
20	24.60	24.38
30	24.82	24.52
80	24.92	24.56

Table 3: Error (%) on CIFAR-100 under different numbers of projections.

Width	$t=1$	$t=2$	$t=4$	$t=8$	$t=16$	$t=20$
Baseline	47.72	38.64	28.13	24.95	24.44	23.77
MHE [12]	36.84	30.05	26.75	24.05	23.14	22.36
HS-MHE [12]	35.16	29.33	25.96	23.38	21.83	21.22
RP-CoMHE	**34.73**	**28.92**	24.39	**22.44**	20.81	20.62
AP-CoMHE	34.89	29.01	**24.33**	22.6	**20.72**	**20.50**

Table 4: Error (%) on CIFAR-100 with different network width.

Network width. We evaluate RP-CoMHE and AP-CoMHE with different network width on CIFAR-100. We use the plain CNN-9 as our backbone network architecture, and set its filter number in Conv1.x, Conv2.x and Conv3.x (see Appendix A) to $16 \times t$, $32 \times t$ and $64 \times t$, respectively. Specifically, we test the cases where $t = 1, 2, 4, 8, 16$. Taking $t = 2$ as an example, then the filter numbers in Conv1.x, Conv2.x and Conv3.x are 32, 64 and 128, respectively. For RP, we set the projection dimension to 30 and the number of projection to 5. For AP, the number of projection is 1 and the projection dimension is set to 30. The results are shown in Table 4. Note that, we use the unrolled optimization in AP-CoMHE. From Table 4, one can observe that the performance gains of both RP-CoMHE and AP-CoMHE are very consistent and significant. With wider network, CoMHE also achieves better accuracy. Compared to the strong results of half-space MHE, CoMHE still obtains more than 1% accuracy boost under different network width.

Network depth. We evaluate RP-CoMHE and AP-CoMHE with different network depth on CIFAR-100. We use three plain CNNs with 6, 9 and 15 convolution layers, respectively. For all the networks, we set the filter number in Conv1.x, Conv2.x and Conv3.x to 64, 128 and 256, respectively. Detailed network architectures are given in Appendix A. For RP, we set the projection dimension to 30 and the number of projection to 5. For AP, the number of projection is 1 and the projection dimension is set to 30. Table 5 shows that both RP-CoMHE and AP-CoMHE can outperform half-space MHE by a considerable margin while regularizing a plain CNN with different depth.

Depth	CNN-6	CNN-9	CNN-15
Baseline	32.08	28.13	N/C
MHE [12]	28.16	26.75	26.90
HS-MHE [12]	27.56	25.96	25.84
RP-CoMHE	26.73	24.39	**24.21**
AP-CoMHE	**26.55**	**24.33**	24.55

Table 5: Error on CIFAR-100 with different network depth. N/C denotes Not Converged.

Effectiveness of optimization. To verify that our CoMHE can better minimize the hyperspherical energy, we compute the hyperspherical energy $\boldsymbol{E}_2$ (Eq. 1) for baseline CNN and CNN regularized by orthogonal regularization, HS-MHE, RP-CoMHE and AP-CoMHE during training. Note that, we compute the original hyperspherical energy rather than the energy after projection. All

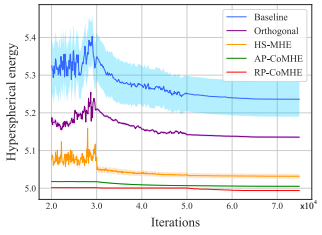

Figure 2: Hyperspherical energy during training. All networks are initialized with the same random weights, so the hyperspherical energy is the same before the training starts.

the networks use exactly the same initialization (the initial hyperspherical energy is the same). The results are averaged over five independent runs. We show the hyperspherical energy after the 20000-th iteration, because at the beginning of the training, hyperspherical energy fluctuates dramatically and is unstable. Interested readers can refer to Appendix G for the complete energy dynamics. From Fig. 2, one can observe that both RP-CoMHE and AP-CoMHE can better minimize the hyperspherical energy. RP-CoMHE can achieve the lowest energy with smallest standard deviation. From the absolute scale, the optimization gain is also very significant. In the high-dimensional space, the variance of hyperspherical energy is usually small (already close to the smallest energy value) and is already difficult to minimize.

ResNet with CoMHE. All the above experiments are performed using VGG-like plain CNNs, so we use the more powerful ResNet [1] to show that CoMHE is architecture-agnostic. We use the same experimental setting in [60] for fair comparison. We use a standard ResNet-32 as our baseline and the network architecture is specified in Appendix A. From the results in Table 6, one can observe that both RP-CoMHE and AP-CoMHE can consistently outperform half-space MHE, showing that CoMHE can boost the performance across different network architectures. More interestingly, the ResNet-32 regularized by CoMHE achieves impressive accuracy and is able to outperform the 1001-layer ResNet by a large margin. Additionally, we note that from Table 4, we can regularize a plain VGG-like 9-layer CNN with CoMHE and achieve 20.81% error rate, which is nearly 2% improvement over the 1001-layer ResNet.

Method	C-10	C-100
ResNet-110 [1]	6.61	25.16
ResNet-1001 [60]	4.92	**22.71**
Baseline	5.19	22.87
Orthogonal [29]	5.02	22.36
SRIP [9]	4.75	22.08
MHE [12]	4.72	22.19
HS-MHE [12]	4.66	22.04
RP-CoMHE	4.59	21.82
AP-CoMHE	**4.57**	**21.63**

Table 6: Error (%) using ResNets.

6.1.2 Large-scale Recognition on ImageNet-2012

We evaluate CoMHE for image recognition on ImageNet-2012 [61]. We perform the experiment using ResNet-18, ResNet-34 and ResNet-50, and then report the top-1 validation error (center crop) in Table 7. Our results show consistent and significant performance gain of CoMHE in all ResNet variants. Compared to the baselines, CoMHE can reduce the top-1 error for more than 1%. Since the computational overhead of CoMHE is almost neglectable, the performance gain is obtained without many efforts. Most importantly, as a plug-in regularization, CoMHE is shown to be architecture-agnostic and produces considerable accuracy gain in most circumstances.

Method	Res-18	Res-34	Res-50
baseline	32.95	30.04	25.30
Orthogonal [29]	32.65	29.74	25.19
Orthnormal [32]	32.61	29.75	25.21
SRIP [9]	32.53	29.55	24.91
MHE [12]	32.50	29.60	25.02
HS-MHE [12]	32.45	29.50	24.98
RP-CoMHE	31.90	29.38	**24.51**
AP-CoMHE	**31.80**	**29.32**	24.53

Table 7: Top-1 center crop error on ImageNet.

Besides the accuracy improvement, we also visualize in Fig. 3 the 64 filters in the first-layer learned by the baseline ResNet and the proposed CoMHE-regularized ResNet. The filters look quite different after we regularize the network using CoMHE. Each filter learned by baseline focuses on a particular local pattern (*e.g.*, edge, color and shape) and each one has a clear local semantic meaning. In contrast, filters learned by CoMHE focuses more on edges, textures and global patterns which do not necessarily have a clear local semantic meaning. However, from a representation basis perspective, having such global patterns may be beneficial to the recognition accuracy. We also observe that filters learned by CoMHE pay less attention to color.

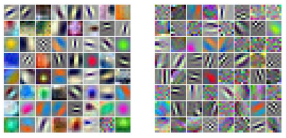

Baseline CoMHE

Figure 3: Visualized first-layer filters.

6.2. Point Cloud Recognition

We evaluate CoMHE on point cloud recognition. Our goal is to validate the effectiveness of CoMHE on a totally different network architecture with a different form of input data structure, rather than achieving state-of-the-art performance on point cloud recognition. To this end, we conduct experiments on widely used neural networks that handles point clouds: PointNet [62] (PN) and PointNet++ [63] (PN++). We combine half-space MHE, RP-CoMHE and AP-CoMHE into PN (without T-Net), PN (with T-Net) and PN++. More experimental details are given in Appendix A. We test the performance on ModelNet-40 [64]. Specifically, since PN can be viewed as 1×1 convolutions before the max pooling layer, we can apply all these MHE variants similarly to CNN. After the max pooling layer, there is a standard fully connected network where we can still apply the MHE variants. We compare the performance of regularizing PN and PN++ with half-space MHE, RP-CoMHE or AP-CoMHE. Table 8 shows that all MHE variants consistently improve PN and PN++, while RP-CoMHE and AP-CoMHE again perform the best among all. We demonstrate that CoMHE is generally useful for different types of input data (not limit to images) and different types of neural networks. CoMHE is also useful in graph neural networks (Appendix J).

Method	PN	PN (T)	PN++
Original	87.1	89.20	90.07
MHE [12]	87.31	89.33	90.25
HS-MHE [12]	87.44	89.41	90.31
RP-CoMHE	87.82	89.69	90.52
AP-CoMHE	**87.85**	**89.70**	**90.56**

Table 8: Accuracy (%) on ModelNet-40.

7. Concluding Remarks

Since naively minimizing hyperspherical energy yields suboptimal solutions, we propose a novel framework which projects the neurons to suitable spaces and minimizes the energy there. Experiments validate CoMHE's superiority.

Acknowledgements. The research is partially supported by NSF BigData program under IIS-1838200, NSF CPS program under CMMI-1932187, and USDOT via C2SMART under 69A3551747124.

References

[1] Kaiming He, Xiangyu Zhang, Shaoqing Ren, and Jian Sun. Deep residual learning for image recognition. In *CVPR*, 2016. 1, 6, 8

[2] Ross Girshick, Jeff Donahue, Trevor Darrell, and Jitendra Malik. Rich feature hierarchies for accurate object detection and semantic segmentation. In *CVPR*, 2014. 1

[3] Jonathan Long, Evan Shelhamer, and Trevor Darrell. Fully convolutional networks for semantic segmentation. In *CVPR*, 2015. 1

[4] Sergey Ioffe and Christian Szegedy. Batch normalization: Accelerating deep network training by reducing internal covariate shift. In *ICML*, 2015. 1, 6

[5] Nitish Srivastava, Geoffrey Hinton, Alex Krizhevsky, Ilya Sutskever, and Ruslan Salakhutdinov. Dropout: A simple way to prevent neural networks from overfitting. *JMLR*, 15(1):1929–1958, 2014. 1

[6] Tim Salimans and Diederik P Kingma. Weight normalization: A simple reparameterization to accelerate training of deep neural networks. In *NIPS*, 2016. 1

[7] Andrew M Saxe, James L McClelland, and Surya Ganguli. Exact solutions to the nonlinear dynamics of learning in deep linear neural networks. *arXiv preprint arXiv:1312.6120*, 2013. 1

[8] Dmytro Mishkin and Jiri Matas. All you need is a good init. In *ICLR*, 2016. 1, 3

[9] Nitin Bansal, Xiaohan Chen, and Zhangyang Wang. Can we gain more from orthogonality regularizations in training deep networks? In *NeurIPS*, 2018. 1, 3, 6, 8

[10] Pau Rodríguez, Jordi Gonzalez, Guillem Cucurull, Josep M Gonfaus, and Xavier Roca. Regularizing cnns with locally constrained decorrelations. *arXiv preprint arXiv:1611.01967*, 2016. 1

[11] Lei Huang, Xianglong Liu, Bo Lang, Adams Wei Yu, Yongliang Wang, and Bo Li. Orthogonal weight normalization: Solution to optimization over multiple dependent stiefel manifolds in deep neural networks. In *AAAI*, 2018. 1

[12] Weiyang Liu, Rongmei Lin, Zhen Liu, Lixin Liu, Zhiding Yu, Bo Dai, and Le Song. Learning towards minimum hyperspherical energy. *NeurIPS*, 2018. 1, 2, 3, 6, 7, 8

[13] J Batle, Armen Bagdasaryan, M Abdel-Aty, and S Abdalla. Generalized thomson problem in arbitrary dimensions and non-euclidean geometries. *Physica A: Statistical Mechanics and its Applications*, 451:237–250, 2016. 2

[14] Matthew Calef, Whitney Griffiths, and Alexia Schulz. Estimating the number of stable configurations for the generalized thomson problem. *Journal of Statistical Physics*, 160(1):239–253, 2015. 2

[15] Y Xiang, DY Sun, W Fan, and XG Gong. Generalized simulated annealing algorithm and its application to the thomson model. *Physics Letters A*, 233(3):216–220, 1997. 2

[16] Y Xiang and XG Gong. Efficiency of generalized simulated annealing. *Physical Review E*, 62(3):4473, 2000. 2

[17] Kenji Kawaguchi, Bo Xie, and Le Song. Deep semi-random features for nonlinear function approximation. In *AAAI*, 2018. 2, 6

[18] Ali Rahimi and Benjamin Recht. Random features for large-scale kernel machines. In *NIPS*, 2008. 2

[19] Zeev Nehari. *Conformal mapping*. Courier Corporation, 2012. 2

[20] Julien Mairal, Francis Bach, Jean Ponce, and Guillermo Sapiro. Online dictionary learning for sparse coding. In *ICML*, 2009. 3

[21] Ignacio Ramirez, Pablo Sprechmann, and Guillermo Sapiro. Classification and clustering via dictionary learning with structured incoherence and shared features. In *CVPR*, 2010. 3

[22] Nan Li, Yang Yu, and Zhi-Hua Zhou. Diversity regularized ensemble pruning. In *Joint European Conference on Machine Learning and Knowledge Discovery in Databases*, 2012. 3

[23] Ludmila I Kuncheva and Christopher J Whitaker. Measures of diversity in classifier ensembles and their relationship with the ensemble accuracy. *Machine learning*, 51(2):181–207, 2003. 3

[24] Lu Jiang, Deyu Meng, Shoou-I Yu, Zhenzhong Lan, Shiguang Shan, and Alexander Hauptmann. Self-paced learning with diversity. In *NIPS*, 2014. 3

[25] Pengtao Xie, Wei Wu, Yichen Zhu, and Eric P Xing. Orthogonality-promoting distance metric learning: convex relaxation and theoretical analysis. In *ICML*, 2018. 3

[26] Pengtao Xie, Jun Zhu, and Eric Xing. Diversity-promoting bayesian learning of latent variable models. In *ICML*, 2016. 3

[27] Pengtao Xie, Aarti Singh, and Eric P Xing. Uncorrelation and evenness: a new diversity-promoting regularizer. In *ICML*, 2017. 3

[28] Michael Cogswell, Faruk Ahmed, Ross Girshick, Larry Zitnick, and Dhruv Batra. Reducing overfitting in deep networks by decorrelating representations. In *ICLR*, 2016. 3

[29] Pau Rodríguez, Jordi Gonzalez, Guillem Cucurull, Josep M Gonfaus, and Xavier Roca. Regularizing cnns with locally constrained decorrelations. In *ICLR*, 2017. 3, 6, 8

[30] Di Xie, Jiang Xiong, and Shiliang Pu. All you need is beyond a good init: Exploring better solution for training extremely deep convolutional neural networks with orthonormality and modulation. *arXiv:1703.01827*, 2017. 3

[31] Weiyang Liu, Yandong Wen, Zhiding Yu, and Meng Yang. Large-margin softmax loss for convolutional neural networks. In *ICML*, 2016. 3

[32] Weiyang Liu, Yan-Ming Zhang, Xingguo Li, Zhiding Yu, Bo Dai, Tuo Zhao, and Le Song. Deep hyperspherical learning. In *NIPS*, 2017. 3, 6, 8

[33] Weiyang Liu, Yandong Wen, Zhiding Yu, Ming Li, Bhiksha Raj, and Le Song. Sphereface: Deep hypersphere embedding for face recognition. In *CVPR*, 2017. 3

[34] Weiyang Liu, Zhen Liu, Zhiding Yu, Bo Dai, Rongmei Lin, Yisen Wang, James M Rehg, and Le Song. Decoupled networks. *CVPR*, 2018. 3, 6

[35] Jiankang Deng, Jia Guo, and Stefanos Zafeiriou. Arcface: Additive angular margin loss for deep face recognition. *arXiv preprint arXiv:1801.07698*, 2018. 3

[36] Hao Wang, Yitong Wang, Zheng Zhou, Xing Ji, Zhifeng Li, Dihong Gong, Jingchao Zhou, and Wei Liu. Cosface: Large margin cosine loss for deep face recognition. *arXiv preprint arXiv:1801.09414*, 2018. 3

[37] Feng Wang, Xiang Xiang, Jian Cheng, and Alan L Yuille. Normface: L2 hypersphere embedding for face verification. *arXiv preprint arXiv:1704.06369*, 2017. 3

[38] Feng Wang, Weiyang Liu, Haijun Liu, and Jian Cheng. Additive margin softmax for face verification. *arXiv preprint arXiv:1801.05599*, 2018. 3

[39] Weiyang Liu, Zhen Liu, James M Rehg, and Le Song. Neural similarity learning. In *NeurIPS*, 2019. 3, 6

[40] Pascal Mettes, Elise van der Pol, and Cees Snoek. Hyperspherical prototype networks. In *NeurIPS*, 2019. 3

[41] Harald Cramér. *Mathematical methods of statistics (PMS-9)*, volume 9. Princeton university press, 2016. 4

[42] Chelsea Finn, Pieter Abbeel, and Sergey Levine. Model-agnostic meta-learning for fast adaptation of deep networks. In *ICML*, 2017. 4

[43] Hanxiao Liu, Karen Simonyan, and Yiming Yang. Darts: Differentiable architecture search. *arXiv preprint arXiv:1806.09055*, 2018. 4

[44] Bo Dai, Hanjun Dai, Niao He, Weiyang Liu, Zhen Liu, Jianshu Chen, Lin Xiao, and Le Song. Coupled variational bayes via optimization embedding. In *NIPS*, 2018. 4

[45] Ian Goodfellow, Jean Pouget-Abadie, Mehdi Mirza, Bing Xu, David Warde-Farley, Sherjil Ozair, Aaron Courville, and Yoshua Bengio. Generative adversarial nets. In *NIPS*, 2014. 4

[46] Yuxin Wu and Kaiming He. Group normalization. In *ECCV*, 2018. 5

[47] Sanjoy Dasgupta and Anupam Gupta. An elementary proof of a theorem of johnson and lindenstrauss. *Random Structures & Algorithms*, 22(1):60–65, 2003. 5

[48] Ata Kaban. Improved bounds on the dot product under random projection and random sign projection. In *KDD*, 2015. 5

[49] Qinfeng Shi, Chunhua Shen, Rhys Hill, and Anton van den Hengel. Is margin preserved after random projection? *arXiv preprint arXiv:1206.4651*, 2012. 5

[50] Juan A Cuesta-Albertos, Antonio Cuevas, and Ricardo Fraiman. On projection-based tests for directional and compositional data. *Statistics and Computing*, 19(4):367, 2009. 5

[51] Robert J Durrant and Ata Kabán. Random projections as regularizers: learning a linear discriminant from fewer observations than dimensions. *Machine Learning*, 2015. 6

[52] Eric P Xing, Michael I Jordan, Stuart J Russell, and Andrew Y Ng. Distance metric learning with application to clustering with side-information. In *NIPS*, 2003. 6

[53] Richard Baraniuk, Mark Davenport, Ronald DeVore, and Michael Wakin. A simple proof of the restricted isometry property for random matrices. *Constructive Approximation*, 2008. 6

[54] Yaniv Plan and Roman Vershynin. One-bit compressed sensing by linear programming. *Communications on Pure and Applied Mathematics*, 2013. 6

[55] Emmanuel J Candès, Justin Romberg, and Terence Tao. Robust uncertainty principles: Exact signal reconstruction from highly incomplete frequency information. *IEEE Transactions on information theory*, 2006. 6

[56] Tianyi Zhou and Dacheng Tao. Godec: Randomized low-rank & sparse matrix decomposition in noisy case. In *ICML*, 2011. 6

[57] Nir Ailon and Bernard Chazelle. Approximate nearest neighbors and the fast johnson-lindenstrauss transform. In *SOTC*, 2006. 6

[58] Moses Charikar, Kevin Chen, and Martin Farach-Colton. Finding frequent items in data streams. *Theoretical Computer Science*, 2004. 6

[59] Andrew Brock, Theodore Lim, James M Ritchie, and Nick Weston. Neural photo editing with introspective adversarial networks. *arXiv preprint arXiv:1609.07093*, 2016. 6

[60] Kaiming He, Xiangyu Zhang, Shaoqing Ren, and Jian Sun. Identity mappings in deep residual networks. In *ECCV*, 2016. 8

[61] Olga Russakovsky, Jia Deng, Hao Su, Jonathan Krause, Sanjeev Satheesh, Sean Ma, Zhiheng Huang, Andrej Karpathy, Aditya Khosla, Michael Bernstein, et al. Imagenet large scale visual recognition challenge. *IJCV*, pages 1–42, 2014. 8

[62] Charles R Qi, Hao Su, Kaichun Mo, and Leonidas J Guibas. Pointnet: Deep learning on point sets for 3d classification and segmentation. In *CVPR*, 2017. 8

[63] Charles Ruizhongtai Qi, Li Yi, Hao Su, and Leonidas J Guibas. Pointnet++: Deep hierarchical feature learning on point sets in a metric space. In *NIPS*, 2017. 8

[64] Zhirong Wu, Shuran Song, Aditya Khosla, Fisher Yu, Linguang Zhang, Xiaoou Tang, and Jianxiong Xiao. 3d shapenets: A deep representation for volumetric shapes. In *CVPR*, 2015. 8